



**STScI** | SPACE TELESCOPE  
SCIENCE INSTITUTE

Instrument Science Report COS 2025-08(v1)

# Measurement and Implementation of a Delta-Geometric Correction for The COS FUV Detector

---

Nick Indriolo<sup>1,2</sup>, Darshan Kakkad<sup>1,3</sup>, Tom Ake<sup>1</sup>, John Debes<sup>1,2</sup>, David French<sup>1</sup>, Sten Hasselquist<sup>1</sup>, David Sahnou<sup>1</sup>

<sup>1</sup> Space Telescope Science Institute, Baltimore, MD

<sup>2</sup> AURA for European Space Agency, STScI, USA

<sup>3</sup> Centre for Astrophysics Research, University of Hertfordshire, Hatfield AL10 9AB, UK

2 July 2025

---

## ABSTRACT

*The geometric distortion correction—one of the earliest steps in the calibration of COS FUV data—enforces a uniform plate scale across the detector such that all digital pixels correspond to the same physical size. The walk correction, which follows the geometric distortion correction, ensures that photons observed at different gain levels are properly aligned on the detector. During the effort to measure X-walk (walk in the dispersion direction) and re-measure geometric distortion, it was determined that coherent, small-scale ( $\leq 5$  pixels) errors in the dispersion direction remained, even after application of new geometric distortion and X-walk corrections. The decision was made to remove these residuals using a delta-geometric correction, to be applied after the initial geometric distortion correction, and before the X-walk correction within the flow of the CalCOS pipeline. Here we describe the motivations for using a delta correction, the data used to measure the correction, and the analysis used to create a new DGEOFILE reference file.*

---

## Contents

1. Introduction . . . . .	2
2. Analysis of Residual Distortions . . . . .	5
2.1 X-interpolation . . . . .	5
2.2 Y-interpolation . . . . .	8
3. Results . . . . .	9
4. Summary . . . . .	10
Acknowledgements . . . . .	11
Change History for COS ISR 2025-08 . . . . .	11
References . . . . .	12

## 1. Introduction

The far ultraviolet (FUV) detector on the Cosmic Origins Spectrograph (COS) consists of two analog detector segments, with the locations of incident photons on each segment measured by a pair of cross-delay lines and digitized to an array of size  $16384 \times 1024$  pixels. While the electronics are tuned so that digital pixels have roughly the same size across the detector, the plate scale in thermally-corrected coordinates is not entirely uniform. This effect is known as integral non-linearity (or geometric distortion) and means that the pixel size varies slightly across the detector. The location assigned to an incident photon also has a dependence on the gain produced by the photon event (quantified as the pulse-height amplitude, PHA, in COS FUV data), an effect known as walk. As usage of the COS FUV detector expanded to more cross-dispersion locations and lower gain levels, it became apparent that improvements could be made to the previous geometric distortion correction, and that the effects of X-walk (walk in the dispersion direction) could no longer be neglected. This motivated the effort by the COS branch to: (1) re-measure the geometric distortion (Kakkad et al. 2025); (2) measure the X-walk (Hasselquist et al. 2025); and (3) deliver new reference files to improve calibrated data products. The project is summarized in Indriolo et al. (2025).

To assess the quality of new geometric distortion and X-walk corrections, a suite of data was chosen to serve as testing metrics. A full description of the testing metrics suite and the analysis employed for quality assessment is given by French et al. (2025). A brief summary of the testing data and analysis is as follows. At each cross-dispersion location where COS FUV data are routinely recorded, spectra containing a large number of emission or absorption features with known wavelengths were identified. In regions sampled by the primary science aperture (PSA) this includes spectra of the emission-line star  $\epsilon$  Eri and of the SMC supergiant AV 75, which has ample foreground

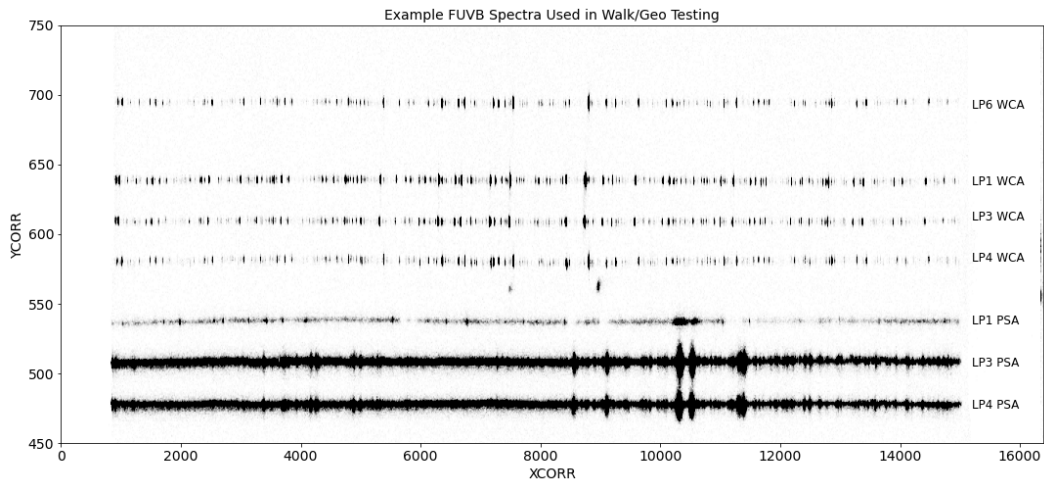


**Figure 1.** The composite 2D spectrograms presented here show the locations of the testing metrics data on FUVB in the (XCORR, YCORR) coordinate system, that has been corrected for thermal effects, geometric distortion, and walk (see Section 2.4 in Soderblom et al. 2022 for more details). Spectra on FUVB have the same relative positions with respect to each other, but fall at different YCORR values than on FUVB. The separate spectra provide sampling in YCORR, while individual emission lines within each spectrum provide sampling in the XCORR direction, and observations at different CENWAVE and FP-POS settings shift those features to provide even greater sampling. These data enable testing of the new geometric distortion and X-walk corrections for a wide range of XCORR and YCORR locations on both detector segments.

absorption lines from the interstellar medium. In regions sampled by the wavelength calibration aperture (WCA) this consists of high signal-to-noise emission spectra of the Pt-Ne hollow cathode lamp within the instrument calibration platform that were observed for the purpose of creating LAMPTAB reference files (e.g., Indriolo et al. 2023). Figure 1 shows the portions of the FUVB detector segment sampled by these data sets taken at different lifetime positions (LPs). These data were calibrated using new geometric distortion and X-walk corrections, and extracted spectra were compared to model spectra (and STIS spectra) with linear dispersion solutions for the WCA (and PSA) region. Differences between the wavelengths assigned by CalCOS and the reference wavelengths for emission/absorption features indicate residual errors within the calibrated data. Figure 2 shows examples of this residual analysis for the same data set with the old geometric distortion correction applied (top panel) and with the new geometric distortion and X-walk corrections applied (bottom panel). While results using the new corrections are better than results using the old corrections (width of the distribution of residuals is narrower; large magnitude residuals near the detector edges are reduced), the pattern of coherent structures is still present across most of the detector. Analysis of the full testing metrics suite of data shows that coherent structures

remain at all cross-dispersion locations on both FUVB and FUVB after application of the newly derived geometric distortion and X-walk corrections.

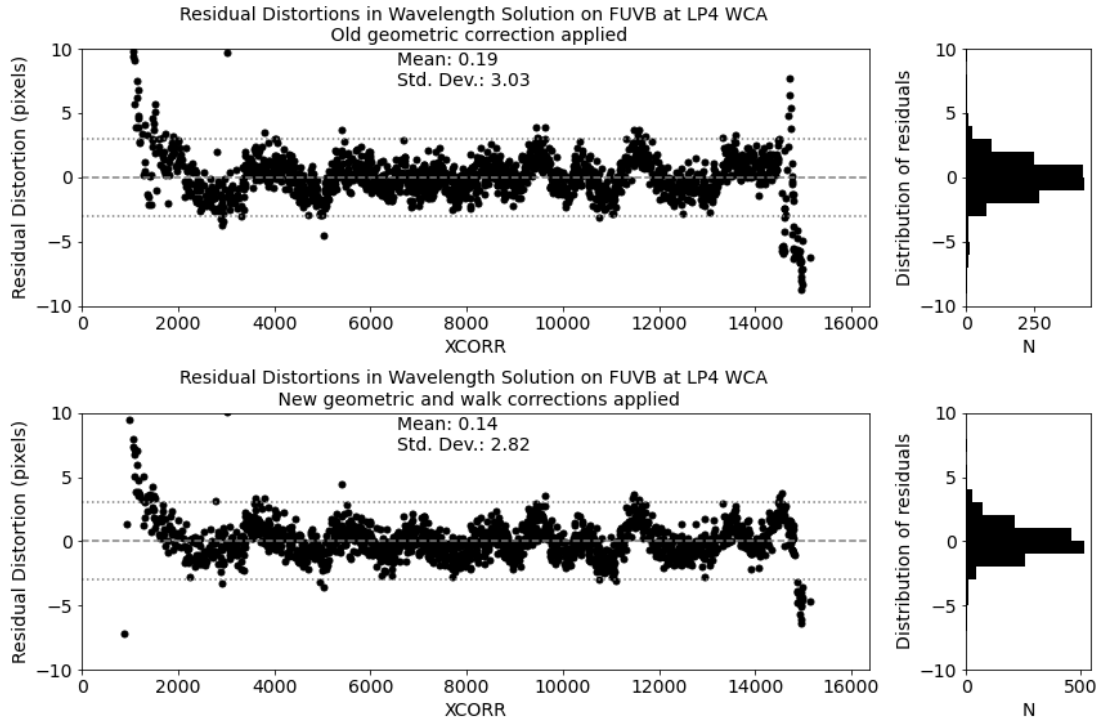


**Figure 2.** This figure shows residual distortions in the dispersion direction at the LP4 WCA region on FUVB for data with the old geometric distortion correction applied (top panel) and with the new geometric distortion and X-walk corrections applied (bottom panel). While the width of the distribution of residuals has decreased with the new reference files, and the magnitude of residuals near the left and right edges has decreased, it is clear that the new corrections do not fix many of the coherent structures within the residuals.

As discussed in Indriolo et al. (2025) the plan to derive new geometric distortion and walk corrections relies on iterating between the two, so that geometric distortion is removed from data used to measure walk, and vice versa. Conceptually, this would separate the effects of walk and geometric distortion and reduce the width of the distribution of residuals with each new iteration. However, the coherent structures in the residuals present a problem to that workflow. Investigation of the pre-launch data used to measure the geometric distortion showed that the coherent structures are not present in those data, so they cannot be removed by the geometric distortion correction. Investigation of the on-orbit data used to measure X-walk showed that the coherent structures are present in the high gain data that are used as a reference, and because X-walk measurements are made relative to those reference spectra the coherent structures also cannot be removed by the walk correction. It is unclear why the residual

structures do appear in the high gain walk dataset but do not appear in the high gain geometric dataset<sup>1</sup>, but the result is a situation where further iteration cannot possibly remove the coherent structures from the testing metrics residuals. The solution to this problem is to add a delta-geometric correction (i.e., small in magnitude with respect to the geometric distortion correction) that is applied following the geometric distortion correction and addresses any residual distortions. The DGEOCORR module in CalCOS was introduced in 2017 with this very intent, but due to complications with implementation the original DGEOFILE reference file (`15c2018f1_dgeo.fits`) has remained full of zeros, and so has no impact on data. By measuring the residual distortions and creating a new DGEOFILE, we will now make use of this pipeline step.

## 2. Analysis of Residual Distortions

Measurement of the residual distortions in data with the new geometric distortion and X-walk corrections applied is “free”, as it is a natural part of the testing metrics analysis described in French et al. (2025). This provides data at seven different cross-dispersion locations on the detector (from top to bottom, LP6 WCA, LP1 WCA, LP3 WCA, LP4 WCA, LP1 PSA, LP3 PSA, LP4 PSA), as shown in Figure 1. The residual distortions shown in the bottom panel of Figure 2 are an example of one of our input data sets. While the data used to measure the delta-geometric correction have been corrected for walk, the delta-geometric correction itself is applied *before* the walk correction in CalCOS. This is not problematic because both the delta-geometric and X-walk corrections are small in magnitude and vary slowly as functions of XCORR. The slow variation means that a correction applied a few pixels away from where it was derived is still “correct” to within the 1-pixel uncertainty introduced by the RANDCORR step.

The DGEOFILE reference file has the same format as the GEOFILE reference file, with the correction stored in four separate image extensions. These contain the  $dx$  and  $dy$  corrections for FUV A and FUV B. We are not applying a delta correction in the y-direction, so both of the  $dy$  images will still be full of zeros. For the x-direction we must first interpolate between measurements at a given cross-dispersion position to fill a row of the  $dx$  image array in XCORR, and then interpolate between the seven different cross-dispersion locations to fill the columns of the  $dx$  image array in YCORR. This process is very similar to that used to create the GEOFILE image arrays from discrete measurements discussed in Kakkad et al. (2025).

### 2.1 X-interpolation

The testing metrics residuals provide 14 different data sets: 7 cross-dispersion locations on both FUV A and FUV B. Interpolation in the x-direction is done separately for each

---

<sup>1</sup>One speculation is a difference between data taken on the ground and on-orbit.

of these data sets using cubic spline fitting to the  $dx$  residuals as a function of XCORR. First, the data are “cleaned” to remove outliers that result from bad measurements (e.g., points at  $(XCORR, YCORR) \approx (900, -7)$  and  $(3000, 10)$  in the bottom panel of Figure 2). Next, the spacing of the nodes for the cubic spline fitting is set based on the density of points in the x-direction. Data sets with higher sampling use a larger number of data points between nodes than data sets with sparser sampling. A list of node densities for each data set is provided in Table 1, and an example of the spline fitting procedure is shown in Figure 3. Due to the sparse sampling of larger fluctuations near the edges of the detector, it was necessary to decrease the distance between nodes on the right edge of FUVB and left edge of FUVB for WCA data sets. Starting with the seventh-to-last node on the right edge of FUVB the number of data points between adjacent nodes was cut in half. The same was done for the left edge of FUVB until reaching the fifth node. This ensures that the rapid, large-scale fluctuations present at some detector edges are properly tracked by the spline fit. Beyond the regions in XCORR where data are available, the spline fit is extrapolated using a constant value equal to the first (last) point in the measured region on the left (right) side of the detector.

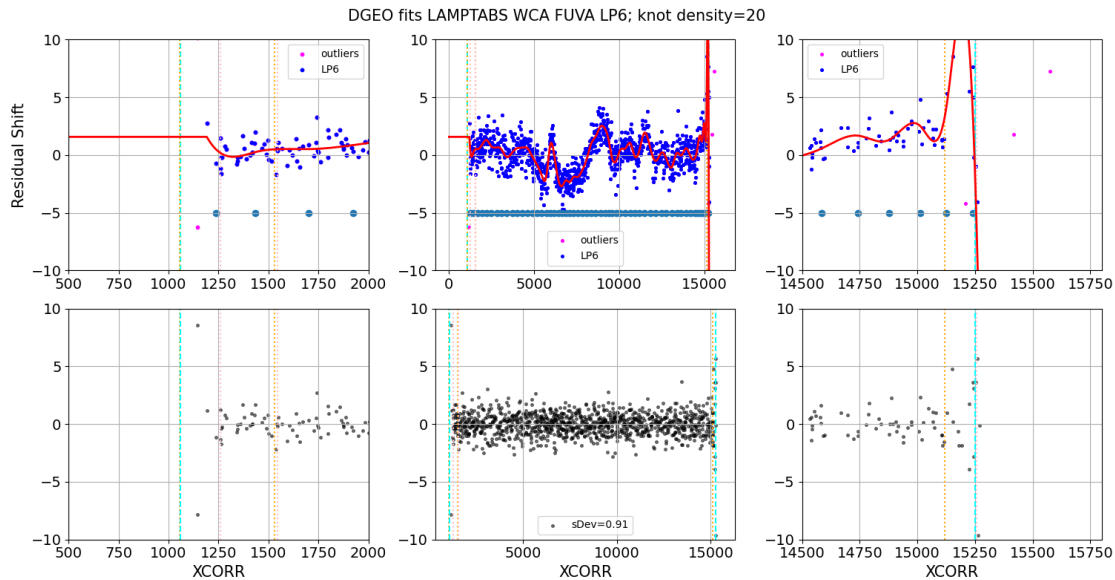


**Figure 3.** This is an example of the cubic spline fitting in the XCORR direction for residual distortions at the LP6 WCA location on FUVB. The middle column shows the full data set, while the left and right columns zoom in on the left and right edges of the detector, respectively. The top row contains the measured distortions as blue points and the spline fit as a red curve. Magenta points mark data points that were excluded from the fitting process as outliers, while large circles at  $-5$  show the locations of the spline nodes. In the bottom row, black points show the difference between the data points and the spline fit.

**Table 1.** Interpolation Parameters

Data Set	Spline Node Spacing		Cross-Dispersion Location (YCORR)	
	FUVA (points)	FUVB (points)	FUVA	FUVB
LP6 WCA	20	20	635	695
LP1 WCA	30	33	588	644
LP3 WCA	25	33	554	614
LP4 WCA	30	33	521	585
LP1 PSA	35	33	484	543
LP3 PSA	20	15	452	510
LP4 PSA	15	10	422	481

Note. — Spline Node Spacing gives the number of measured data points in between adjacent nodes for cubic spline fitting in the  $x$ -direction. These were determined by trial and error to avoid over-fitting the data, while still capturing small-scale coherent structures. As mentioned in Section 2.1, the separation between nodes was decreased in some cases near the edges of the detector. Cross-Dispersion Location gives the YCORR location assigned to each data set for interpolation in the  $y$ -direction. These are the mean values for all B\_SPEC entries for standard modes (G130M 1291–1327 and G160M 1577–1623) within the XTRACTAB reference file at a given LP.

## 2.2 Y-interpolation

The result of fitting all 7 data sets on FUVA is shown in Figure 4. While many of the narrow features are unique to one y-location, some of the broader features (e.g.,  $11000 <XCORR < 12000$ ) do appear at most y-locations. At this point, the  $dx$  image arrays are only populated (by the spline fits) at the 7 rows where the underlying data sets were obtained,<sup>2</sup> listed in Table 1. To fully populate the  $dx$  image in the y-direction, we must also interpolate between the various spline fits.

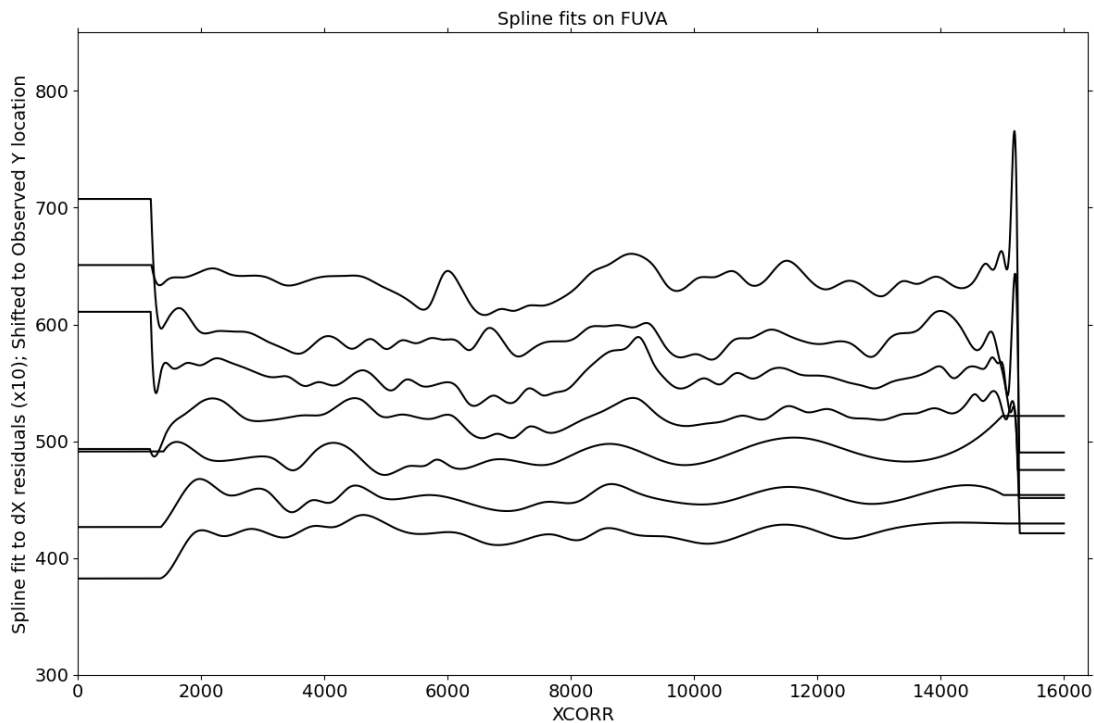


**Figure 4.** This shows the spline fits to the seven different data sets on FUVA. The  $dx$  correction given by each curve has been multiplied by 10 to more clearly show the structures, and then shifted to the y-locations given in Table 1 to represent where the underlying measurements were obtained on the detector.

Several different methods were considered for interpolation in the y-direction, including: cubic spline fitting forced to pass through the measurements (CS); inverse distance weighting (IDW); linear piece-wise between the measured rows (LPW); and a linear fit (LF). Each method presents certain advantages and disadvantages; an example of the IDW and LF methods is shown in Figure 5. The CS, IDW, and LPW methods all keep the exact results from the spline fitting in the x-direction at the appropriate y-

<sup>2</sup>While spectra taken with the G130M and G160M gratings project to slightly different y-locations on the detector (5–10 pixels apart), because the cross-dispersion profiles are also of order 10 pixels wide, we decided to register all data at a given LP to the same YCORR location.

location. This makes these methods very good at correcting the data used to measure the residual distortions. However, all of these methods can also have rapid changes in  $dx$  between the y-locations where the measurements were made. For observations made at cross-dispersion locations between the data sets, this can lead to incorrect shifts being applied. In some cases, the CS fit even goes well beyond the input data points, introducing larger  $dx$  corrections than what are within the original data set. The LF method does not retain the exact results from spline fitting in the x-direction, so it does not “perfectly” correct the data used to measure the residual distortions. If one of the x-direction spline fits differs significantly from those around it, the residual distortions at that location will not be improved by this method. The LF method does have the advantage, however, of not introducing any rapid changes in  $dx$  as a function of YCORR. This means it will not introduce artifacts for observations taken in between the locations of the data sets. After several tests, we decided to proceed using the linear fit method. While it does not perfectly correct the data used to measure the residual distortions, the stability in between the YCORR locations of the input data sets is vital. This is because the G130M, G160M, and G140L gratings all project spectra to slightly different y-locations on the detector, and because the cross-dispersion profiles of spectra observed through the PSA are tens of pixels wide. The final reference file images for the delta-geometric  $dx$  corrections on FUVB and FUVB are shown in Figure 6.

### 3. Results

In order to test the new delta-geometric correction, we first applied it to the the testing metrics data suite. This amounts to testing the correction on the data from which it was derived, but is a useful step in confirming that the correction works as intended. Figure 7 shows the same data set presented in Figure 2, but this time the data had the new geometric distortion, delta-geometric, and X-walk corrections applied. The width of the distribution of residuals has again decreased (from  $\sigma = 2.82$  to  $\sigma = 2.62$ ), and the magnitudes of the coherent structures have been reduced. This demonstrates that the delta-geometric correction successfully removes a portion of the residual distortion on the detector.

A second important test is to confirm that the delta-geometric correction works well on data that were not used in the derivation process. Because emission lines in the Pt-Ne spectra provide better sampling than emission lines in the spectrum of  $\epsilon$  Eri, in regions where the PSA and WCA overlap, only the WCA data were used to derive the delta-geometric correction. As a result,  $\epsilon$  Eri observations taken at LP6 provide an independent data set with which to test the delta-geometric correction. Figure 8 shows the analysis of these data, both before and after application of the new corrections. It is clear that the width of the distribution of residuals significantly decreases following application of the new reference files (from  $\sigma_{old} = 1.71$  to  $\sigma_{new} = 0.89$ ), and that coherent structures have been removed by the delta-geometric correction. This test demonstrates that the delta-geometric correction works on data that were not used in

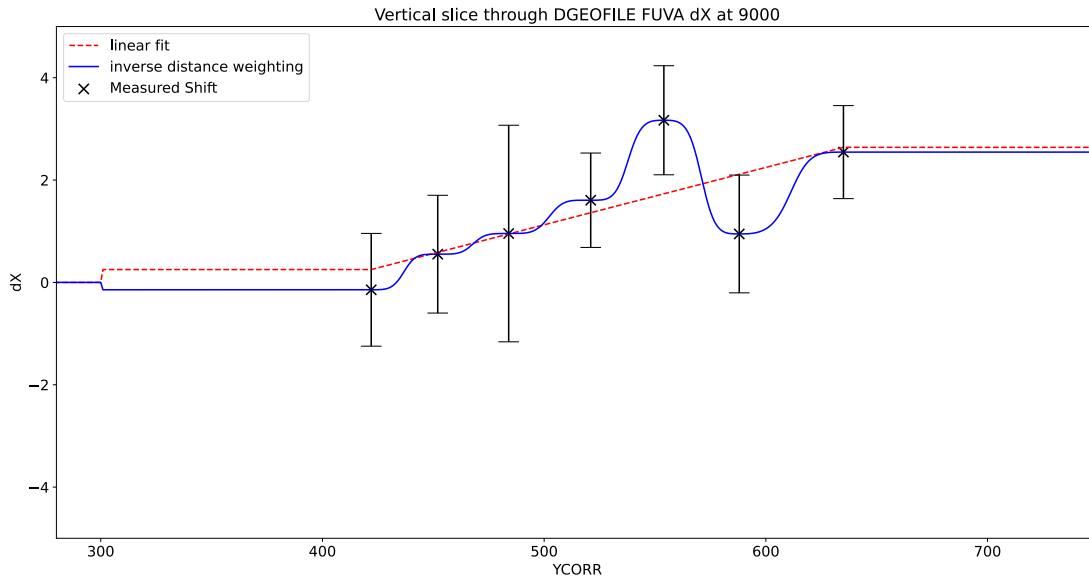


**Figure 5.** Example showing different methods of interpolating between the y-locations where spline fits were done to the data sets in the x-direction. Black crosses show the  $dx$  correction at the y-locations of the 7 data sets for  $XCORR = 9000$  on FUVA. The red dashed line is a linear fit to the points, while the blue curve uses inverse distance weighting (Bouhlef et al. 2019). Outside of the YCORR range with measurements,  $dx$  is set to a constant value, equal to the last interpolated value in the measured region. These fits populate a single XCORR column of the DGEOFILE  $dx$  image array, and this same analysis is done for all XCORR.

deriving the correction, and that were not observed at the same y-location as the data used in deriving the correction.

## 4. Summary

Residual distortions in the suite of testing metrics data were used as input to derive a new delta-geometric correction for the COS FUV detector. The correction only applies in the x-direction (i.e., there is no delta-geometric  $dy$  correction), and is primarily intended to remove coherent structures that were found in the testing metrics residuals. Application of the delta-geometric correction, in addition to the new geometric distortion and X-walk corrections, results in decreased widths of the distribution of residuals and decreased magnitudes of the coherent structures. This decreases the relative error in wavelengths assigned to portions of the spectrum recorded at different x-locations from about  $20 \text{ km s}^{-1}$  to about  $10 \text{ km s}^{-1}$  for medium resolution modes.

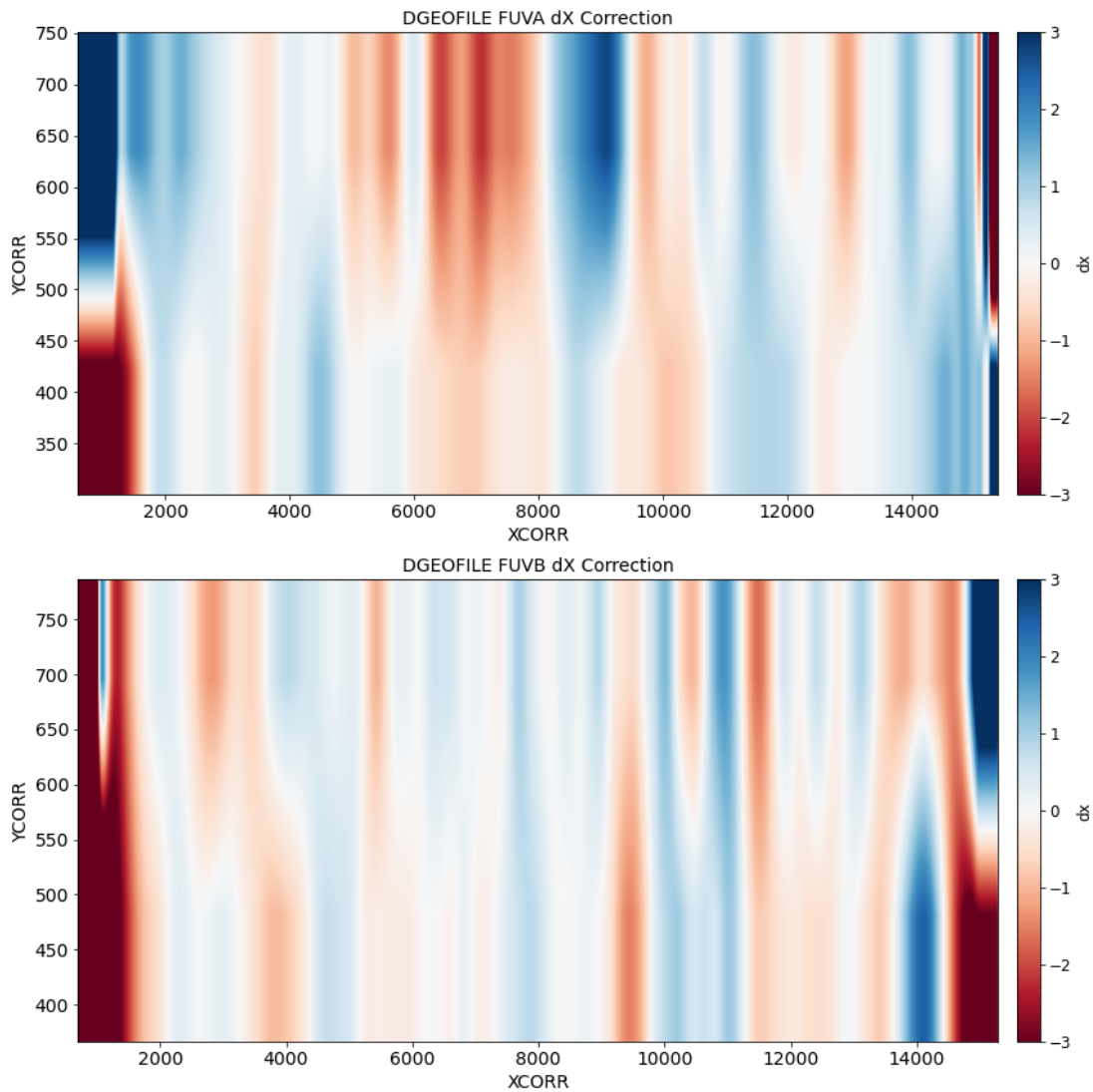


**Figure 6.** These are the final delta-geometric correction  $dx$  image arrays for FUVA (top) and FUVB (bottom). Over most of the detector the magnitude of the correction is less than 3 pixels, with larger corrections only necessary at the left and right edges of both segments.

## Acknowledgements

The authors would like to acknowledge S. V. Penton and J. White for their contributions to this effort while working at STScI.

## Change History for COS ISR 2025-08

Version 1: 2 July 2025- Original Document

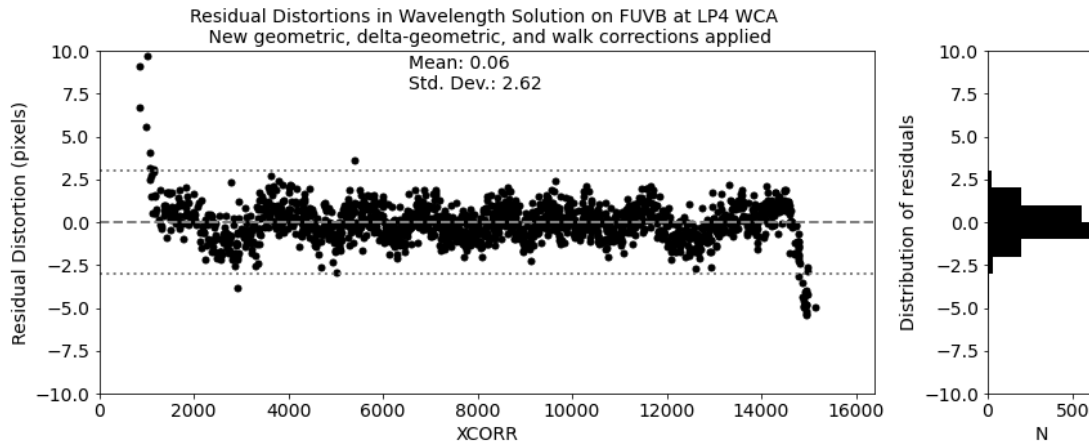


**Figure 7.** Same as Figure 2, but now with the delta-geometric correction also applied to the data used in the testing metrics analysis. Coherent structures in the residuals are reduced, but not fully removed, due to the decisions discussed in Section 2.2. The standard deviation of the residual distribution is 2.62 pixels here, compared to 2.82 pixels when only the new geometric distortion and walk corrections are applied, and 3.03 pixels for the old geometric distortion correction.

## References

- Bouhleb, M. A., et al. 2019, *Advances in Engineering Software*, pp.102662, *A Python surrogate modeling framework with derivatives*
- French, D., et al. 2025, COS ISR 2025-xx *Testing metrics* (In Preparation)
- Hasselquist, S., et al. 2025, COS ISR 2025-10, *Determining X-Walk Corrections for the COS FUV Detector*
- Indriolo, N., et al. 2023, COS ISR 2023-09, *Creation of the LAMPTAB reference file for use at Lifetime Position 6*
- Indriolo, N., et al. 2025, COS ISR 2025-07, *An Overview of Improvements to the COS FUV Geometric Distortion and Walk Corrections*
- Kakkad, D., et al. 2025, COS ISR 2025-09, *A Revised Geometric Distortion Correction for the Far-Ultraviolet Detector of the Cosmic Origins Spectrograph*
- Soderblom, D., et al. 2022, *COS Data Handbook*, Version 5.1, (Baltimore: STScI).

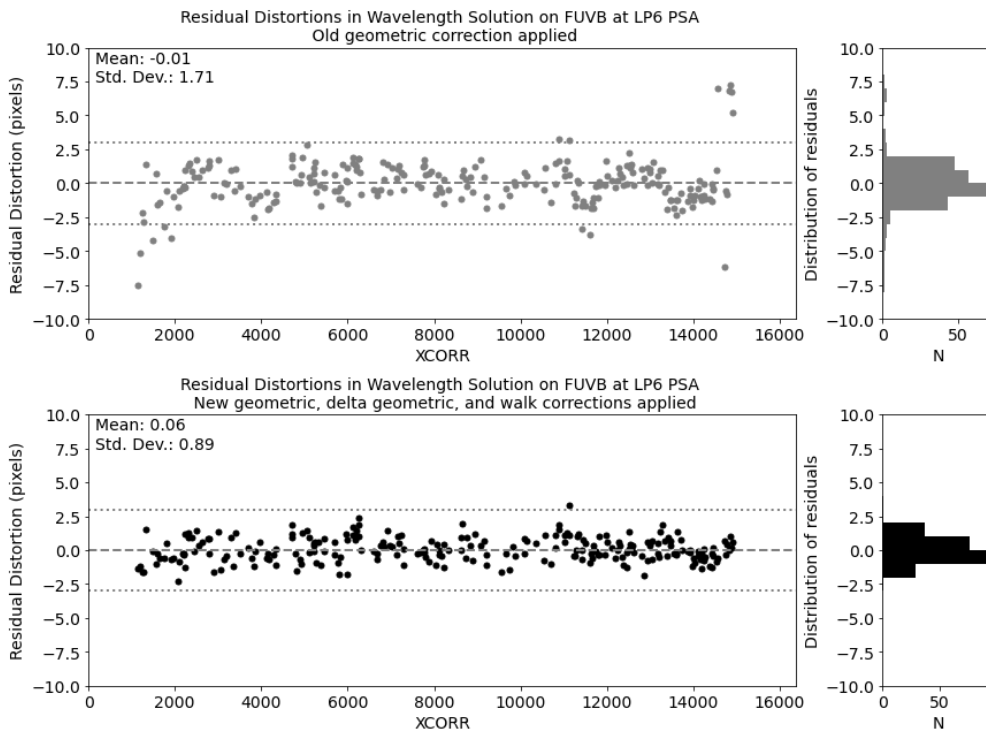


**Figure 8.** Similar to Figures 2 and 7, but here the testing metrics analysis has been done using observations of the emission line star  $\epsilon$  Eri taken at the LP6 PSA region. The top panel shows residuals using the old geometric distortion correction, and the bottom panel shows residuals using the new geometric distortion, delta-geometric, and X-walk corrections.